

JGR Solid Earth

RESEARCH ARTICLE

10.1029/2019JB018147

Key Points:

- Strong ground motion from the 610-km deep M_w 8.3 Sea of Okhotsk earthquake extended from regional to teleseismic distances
- Largest shaking in Japan at distance 2,000 km produced by near caustics of S triplications from the deep event and interactions with slab
- Teleseismic felt reports in continents are due to multiple long-period S reflections and S -PL waves in the continental crust

Supporting Information:

- Supporting Information S1
- Movie S1
- Movie S2
- Movie S3

Correspondence to:

T. Furumura,
furumura@eri.u-tokyo.ac.jp

Citation:

Furumura, T., & Kennett, B. L. N. (2019). The significance of long-period ground motion at regional to teleseismic distances from the 610-km deep M_w 8.3 Sea of Okhotsk earthquake of 24 May 2013. *Journal of Geophysical Research: Solid Earth*, 124, 9075–9094. <https://doi.org/10.1029/2019JB018147>



Received 6 JUN 2019

Accepted 2 AUG 2019

Accepted article online 09 AUG 2019

Published online 30 AUG 2019

The Significance of Long-Period Ground Motion at Regional to Teleseismic Distances From the 610-km Deep M_w 8.3 Sea of Okhotsk Earthquake of 24 May 2013

T. Furumura¹  and B. L. N. Kennett² 

¹Earthquake Research Institute, The University of Tokyo, Tokyo, Japan, ²Research School of Earth Sciences, The Australian National University, Canberra, ACT, Australia

Abstract The 24 May 2013 earthquake beneath the Sea of Okhotsk (610 km, M_w 8.3) produced significant ground motion across the whole span of the Japanese islands, from 1,300- to 4,200-km epicentral distance. The largest shaking was concentrated along the back-arc side of the subduction zone, which is the opposite of the normal pattern for deep earthquakes in the Pacific slab. Observations from the dense Hi-net and F-net arrays across Japan show that the largest shaking in northern Japan (near 2,000-km epicentral distance) was caused by near-caustic S waves, with triplication of upgoing and downgoing waves from the deep source and reflected waves from the 660-km discontinuity. Three-dimensional finite difference method simulations confirm that the antiwaveguide effect of the high-wave speed slab is to push the zone of larger intensity 300 km farther to south than might be expected. The S wavefront distorted by the slab has near-critical incidence at the free surface producing large sP and generating shear-coupled PL (s -PL) waves with period >3 s. With increasing epicentral distance the S incident angle exceeds critical, then total sS reflection creates large ground motion at large distance ($>3,000$ km) and even farther ($>6,000$ km) with sSS . The propagation of sS , sSS linking to sS -PL, and sSS -PL wave trains is very efficient in continental structures with thicker crust. The felt reports at large (4,000–8000 km) distances from the 2013 Sea of Okhotsk earthquake can be explained by lengthy, long-period ground motion in the continental environment with amplification in sedimentary basins and in tall buildings.

1. Introduction

The largest known very deep earthquake occurred in the Pacific slab beneath the Sea of Okhotsk, west of Kamchatka on 24 May 2013 (610 km, M_w 8.3) and produced large shaking across the Japanese islands (Figure 1a). The largest shaking intensity 3 on the Japan Meteorological Agency scale (max 7) was reported in northern Hokkaido (epicentral distance of 1,400 km) and in northern Tohoku (2,000 km). The area of felt reports (intensity ≥ 1) extends to southern Kyushu 3,500 km away from the epicenter (Figure 1a). We will refer to this event as the *2013 Sea of Okhotsk earthquake*.

Usually, moderately deep (<100 – 200 km) earthquakes in the subducting Pacific slab, observed in the epicentral distance range out to 2,000 km, produce larger intensity over the fore-arc side of the Japan trench subduction zone, extending from Hokkaido to Kanto (Tokyo; see, e.g., Figures 1b and 1c). The ground motion is characterized by lengthy high-frequency P and S wave trains due to multiple forward scattering in the heterogeneous subducted slab (Furumura & Kennett, 2005, 2008). Such a slab waveguide effect is only efficient at high frequencies with wavelengths shorter than the scale of heterogeneity in the slab.

The intensity pattern for the 2013 Sea of Okhotsk earthquake was different. There was larger intensity along the Japan Sea side, which is the opposite of the normal pattern for deep earthquakes in the Pacific slab (Figures 1b and 1c). There are two separate zones of larger ground motion in northern Hokkaido and in Tohoku. The observations from Hi-net and F-net (National Research Institute for Earth Science and Disaster Resilience, 2019) across the Japanese islands indicate that the larger intensity was produced by long wave trains of relatively low frequency (<1 Hz) signals following the S wave.

In this study, we investigate the cause of the peculiar low-frequency (long-period) wavefield and the pattern of intensity developed by this large and very deep 2013 Sea of Okhotsk event. We use the dense Hi-net and F-net records across Japan and global broadband seismograph data (IRIS DMC; Incorporated Research

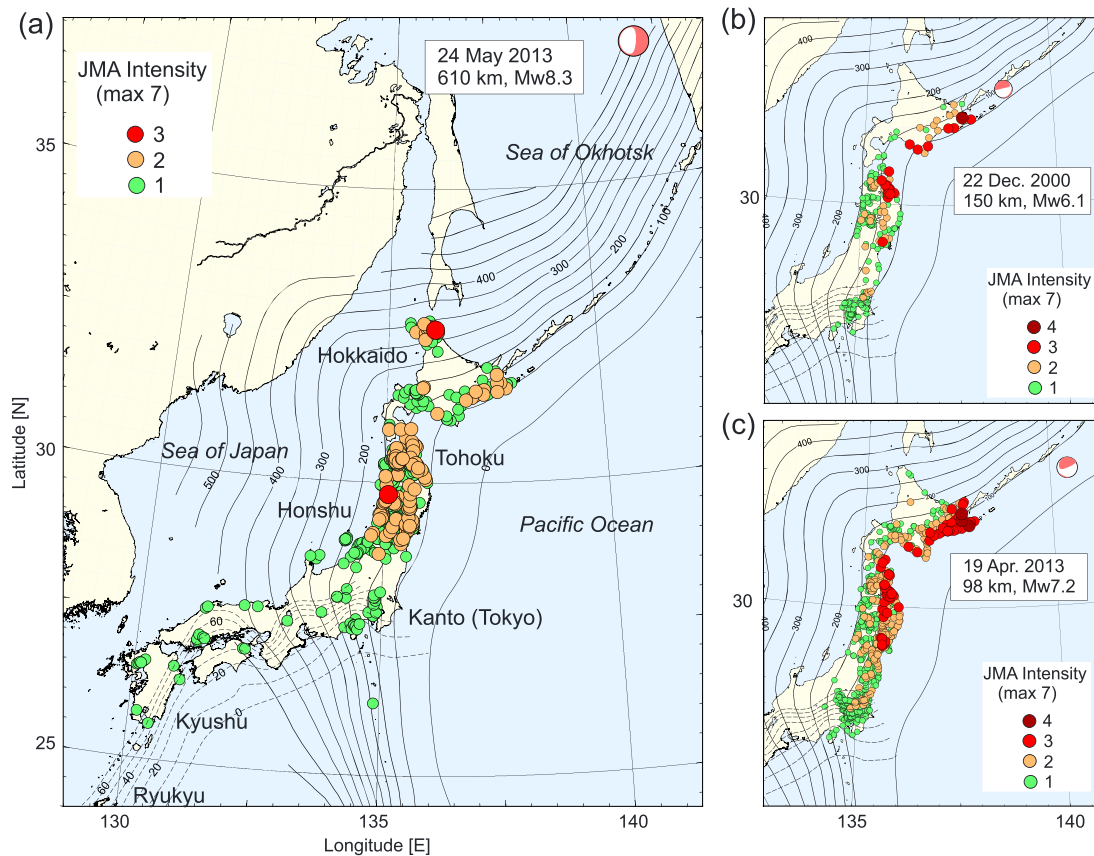


Figure 1. Shaking intensity on the Japan Meteorological Agency scale for (a) 24 May 2013 Sea of Okhotsk earthquake (610 km, M_w 8.3), (b) 22 December 2000 Kurile islands earthquake (150 km, M_w 6.1), and (c) 19 April 2013 Kurile islands earthquake (98 km, M_w 7.2). The isodepth contours of the subducting Pacific slab (continuous line with 50-km interval) and Philippine Sea slab (dashed lines with 10-km interval) are plotted.

Institutions for Seismology, Data Management Center). The observations are complemented by 3-D finite difference method (FDM) simulations of seismic wave propagation with heterogeneous crust and mantle structure including the Pacific Plate subduction zone. We show that the large shaking observed in Tohoku was caused by near caustics in the S waves due to the triplication of upgoing and downgoing S wave from the deep (610 km) source and interactions with the 660-km discontinuity. The S wavefronts associated with the triplication are modified by the presence of the high-wave speed Pacific slab and so are displaced 300 km farther south from the situation without a slab. The large S wave produces strong S -to- P (sP) conversion at the free surface with near-critical incidence. The conversions can travel several hundred kilometers by PmP reflections in the crustal waveguide; they give rise to long-period (3–10 s) shear-coupled PL waves (s-PL) with interaction to upcoming S wave into the crust. This wave train comprising the set of sP, S , and s-PL phases is the major cause of the large and long-duration long-period ground motions across Japan.

Another striking feature of this large, very deep earthquake was that shaking was reported at very large distances. Felt reports come from Dubai, northern India, and California, and in Moscow, 6,000 km away from the epicenter (U.S. Geological Survey (USGS), 2013; Kuge, 2015). Such an anomalously large felt area had also been reported during the deep 1994 Bolivia earthquake (M_w 8.3; 637 km) in North America, as far as 8,680 km from the epicenter (Anderson et al., 1995). By examining the teleseismic records of the 2013 Sea of Okhotsk earthquake, we show that the large ground motions observed at distant continental sites are dominated by lengthy, long-period (>3 s) ground motions, which consist of multiple sS, sSS reflections with long sS-PL and sSS-PL wave trains. The nature of the sS and sSS phases is significantly influenced by the zone of reflection near the source and the subsequent travel path. S reflection is very efficient in the continental environment with thicker crust. The felt reports at very distant continental sites can be explained by the long-period ground motions, lasting several minutes, with amplification by sedimentary basins of populated centers and structural amplifications for tall buildings.

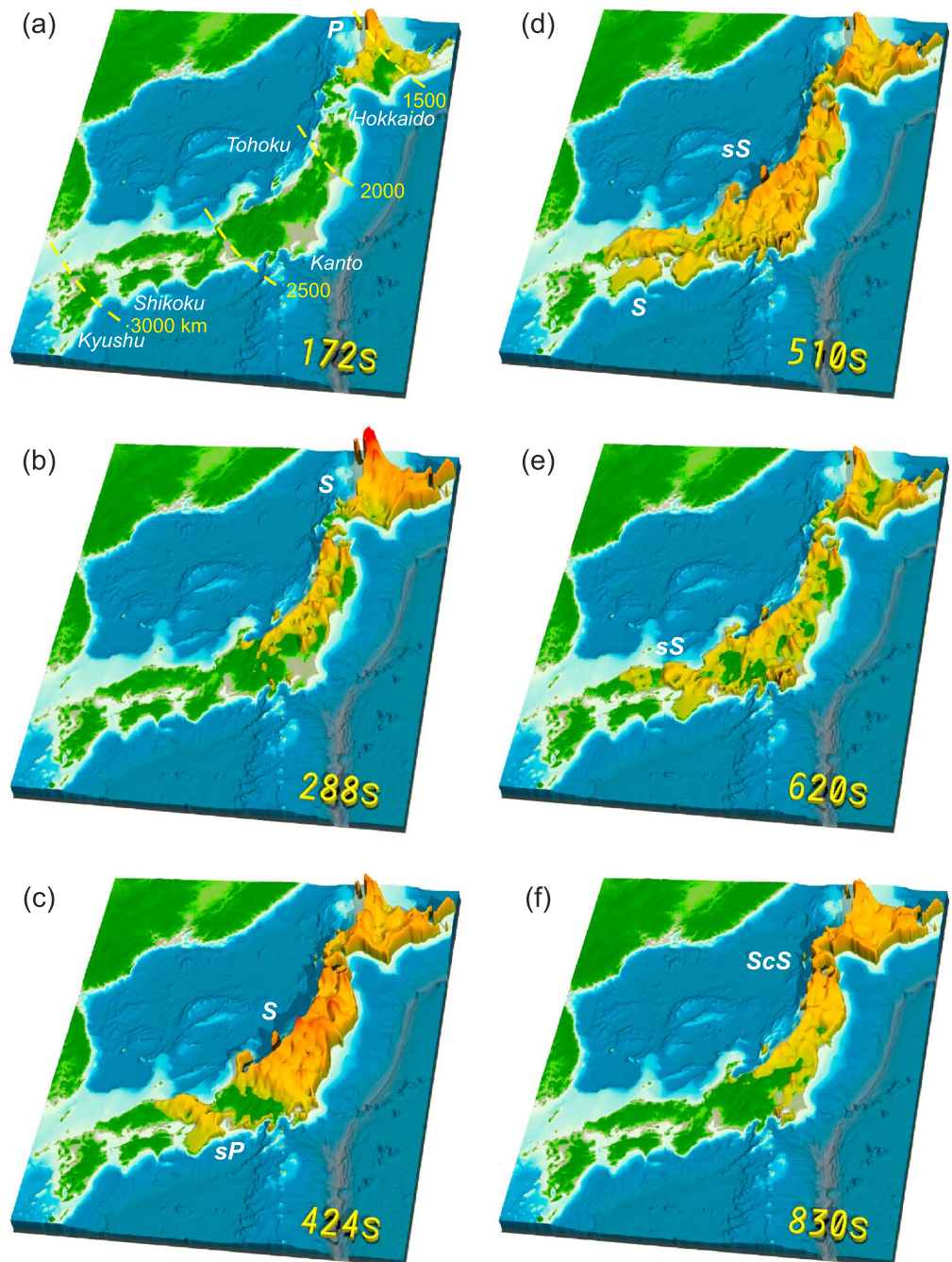


Figure 2. Visualized ground motions for the 2013 Sea of Okhotsk earthquake at 172, 288, 424, 510, 620, and 830 s from the earthquake initiation, obtained by the interpolation of dense Hi-net and F-net records. The strength of horizontal ground velocity motion is visualized by the height and color of the wavefront. Major phases are indicated (also, see Movie S1).

2. Regional Wave Propagation From the 2013 Sea of Okhotsk Earthquake

2.1. Visualization of Seismic Wavefield

The pattern of strong ground motion across Japan for the 2013 Sea of Okhotsk earthquake can be visualized from observed ground motions exploiting continuous records from the high-density Hi-net array and broadband F-net stations. The Hi-net records are adjusted by applying the response-correction filter of Maeda et al. (2011) to produce a broadband record comparable to an STS-2 seismometer. Since the Hi-net sensors are installed in boreholes, and the F-net in vaults, the effect of site amplification is small.

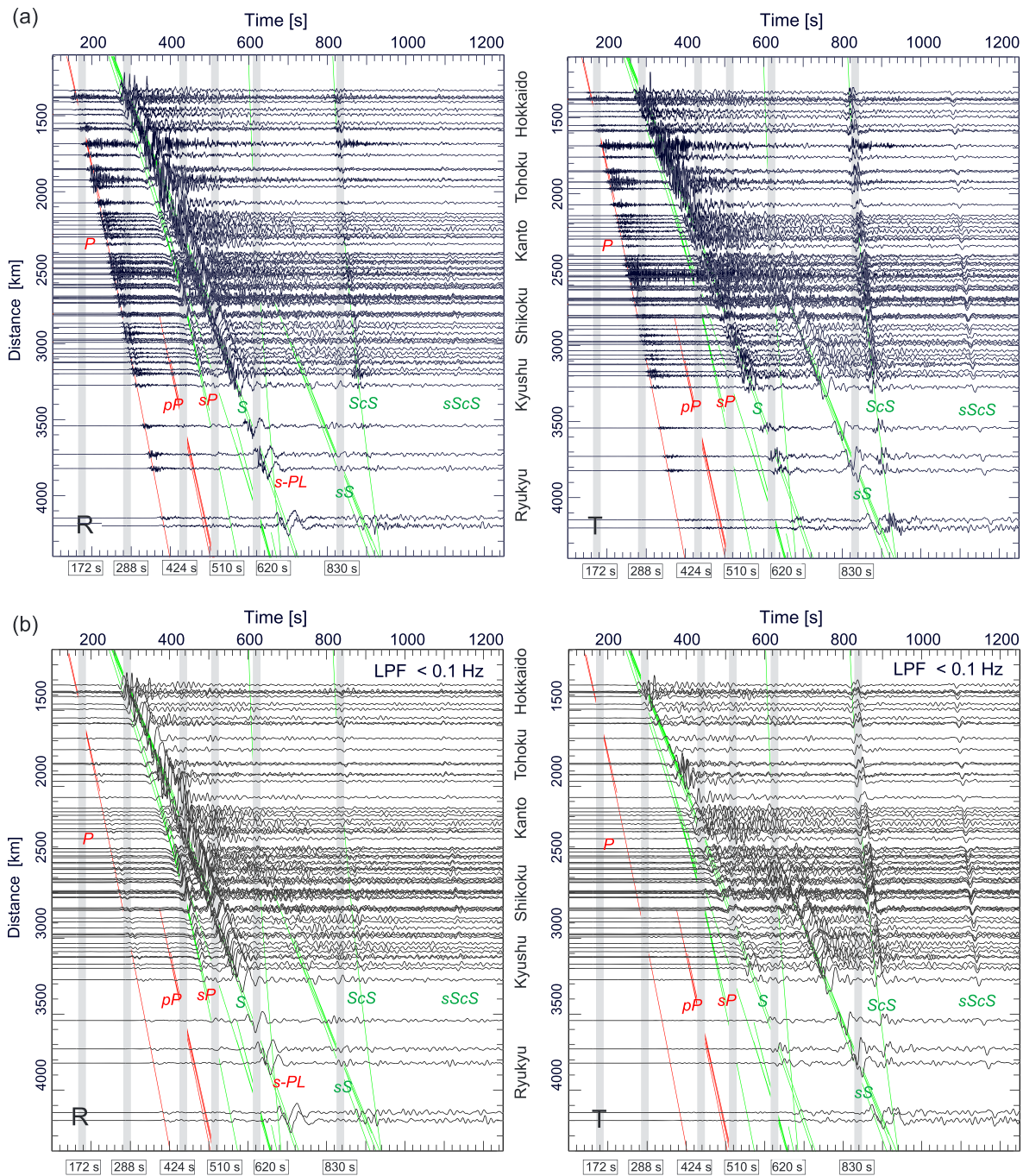


Figure 3. (a) Record sections for radial (R) and transverse (T) component ground velocity for the 2013 Sea of Okhotsk earthquake obtained by the F-net broadband station over Japanese islands. Light gray bands correspond to the time windows used for the snapshots displayed in Figure 2. (b) Low-pass-filtered ($f < 0.1$ Hz) record sections for R and T component ground velocity.

Figure 2 shows the spread of ground motion across Japan as a function of time. The images are obtained by interpolation of horizontal ground motion for the 586 Hi-net and 73 F-net stations on the Japanese mainland for epicentral distances between 1,300 and 3,200 km (see also Movie S1 in the Supporting Information). The records from the F-net stations extend farther to the Ryukyu islands for epicentral distance up to 4,200 km. In each snapshot in Figure 2, the strength of ground velocity is indicated by the height and color (bright orange to dark red) of the wavefront. Figure 3a displays the record section of radial (R) and transverse (T) components of the F-net records, where major phases are marked. A low-pass-filtered ($f < 0.1$ Hz) record

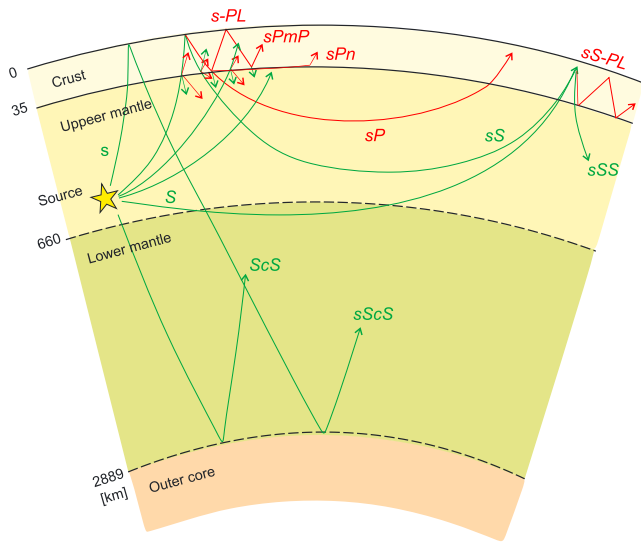


Figure 4. Schematic illustration of the raypaths for major seismic phases from a very deep source: upgoing *S* wave (*s*), downgoing *S* wave (*S*), surface reflected *sS* and *sP*, *sPn* waves, and multiple *sPmP* reflections in the crust, and core-reflected *ScS* and *sScS* are marked. Horizontally traveling *sPmP* multiples in the crust couple with the incoming *S* wave (*s*) develop the *s-PL* phase.

section is also shown in Figure 3b to eliminate slab guided high-frequency waves and to emphasize low-frequency wavefield. A schematic illustration of the raypaths for major phases from the deep source to regional distances is presented in Figure 4.

The first snapshot of the wave propagation, at 172 s after earthquake initiation, shows the beginning of shaking in the north of Hokkaido 1,300 km from the epicenter with upcoming *P* wave from the deep source. By 288 s large ground motion from the upcoming *S* wave has arrived. The *P* and *S* ground motions weaken as they leave northern Hokkaido. Yet, the amplitude recovers again in Tohoku producing a large peak near Akita at an epicentral distance of 2,000 km (424-s snapshot).

Comparison with the record section of *R* component ground velocity (Figure 3) shows that the precursor to the *S* wave, which emerges at epicentral distance greater than 2,000 km and travels over southwestern Japan at the higher *P* wave speed, is the *S*-to-*P* converted (*sP*) wave at the free surface (424-s snapshot). After 510 s from the earthquake, the reflected *S* wave in the Sea of Okhotsk (*sS* wave) creates large ground motion in Honshu, for epicentral distances over 2,500 km. Later, the arrival of the *ScS* core phase (830 s), reflected back from the core/mantle boundary at a nearly vertical angle, flashes across the Japanese islands with a very high apparent wave speed and is followed by *sScS* at much later time.

The sequence of snapshots in Figure 2 suggests that the observed strong ground motions over Japanese islands during the 2013 Sea of Okhotsk earthquake was produced not only by a spike of upcoming *S* body waves but also by the continuous arrival of *sP* and *sS* reflections and *ScS* and *sScS* core phases, etc. The

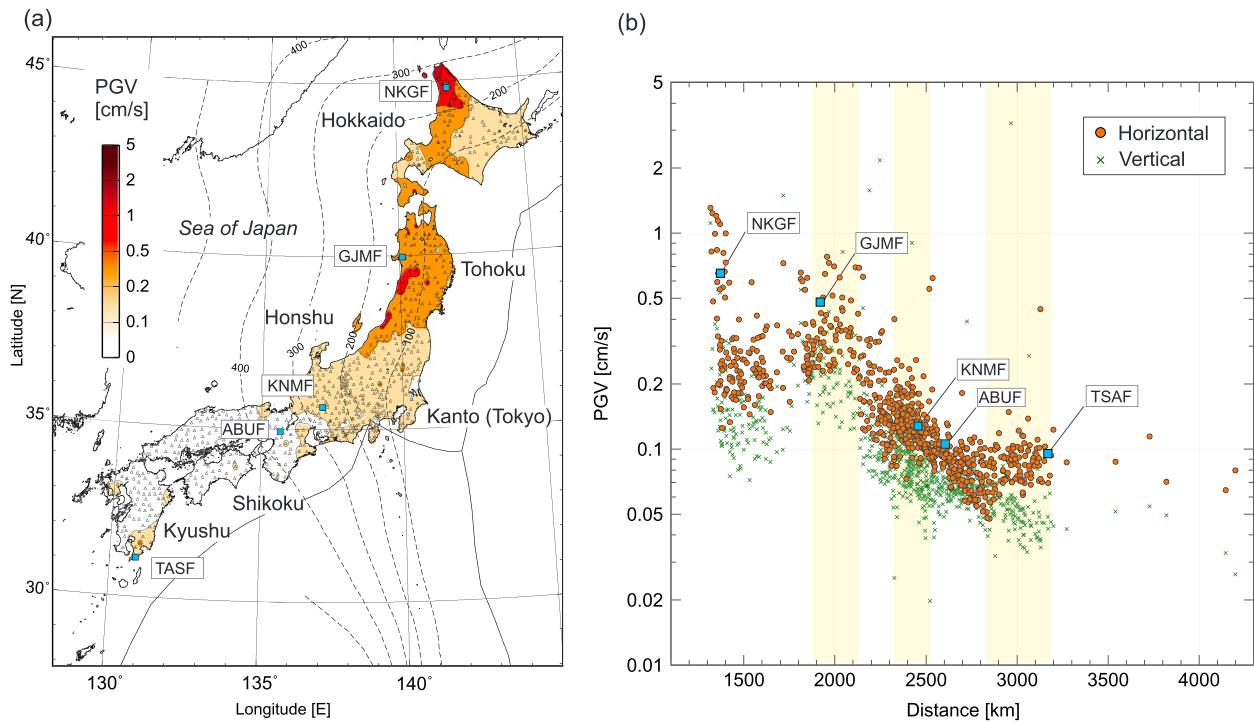


Figure 5. (a) Peak ground velocity (PGV) for horizontal motion for the 2013 Sea of Okhotsk earthquake obtained by interpolation of Hi-net and F-net records. Blue squares represent the F-net stations whose waveforms are shown in Figure 6. (b) Attenuation of PGV of horizontal (orange circles) and vertical (green crosses) motions as a function of epicentral distance obtained from F-net and Hi-net records. Light yellow bands denote the area of locally increased PGV in epicentral distances around 2,000 and 2,400 km, and over 2,800 km.

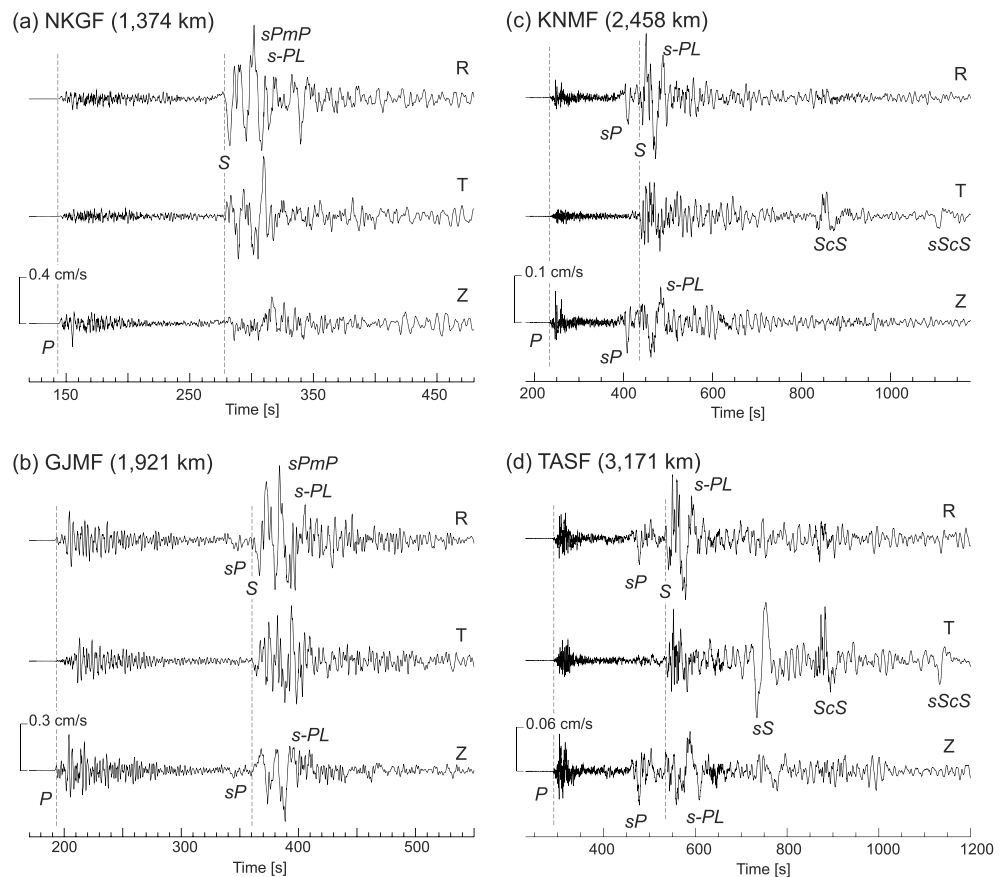


Figure 6. Three-component ground velocity records for radial (R), transverse (T), and vertical (Z) motions recorded at the F-net stations; (a) NKGf, (b) GJMF, (c) KNMF, and (d) TASF (see Figure 5 for locations). Also, see record at station ABUF in S3 of the Supporting Information. Major phases are marked.

composite effect is broad shaking of Japanese islands for several minutes. The record sections show the contrast between the high-frequency of upcoming P and S body waves from the deep source and ScS core phase (Figure 3a) and the relatively low frequency sP , sS , and $sScS$ phases (Figure 3b). The loss of higher frequencies in sP and sS is enhanced by long-distance propagation in the low- Q mantle lid. Significant converted sP phases from upgoing S waves are a distinctive feature of deep earthquakes around the Japanese islands (see Kennett & Furumura, 2019).

In the R record section in Figures 3a and 3b a moderately long period (5–10 s) sP appears before S with the faster mantle P wave speed traveling beneath the Moho. This sP_n phase is observed at distances greater than 2,000 km and has large amplitude at 2,500–3,500 km. The long-period sS reflection in larger (>2,500 km) epicentral distance is very large on the T component, because no energy is lost to P on reflection.

The upcoming S and reflected sS waves are followed by a weakly dispersed, long-period (>10 s) wave train—the shear-coupled PL wave (S -PL; Oliver, 1961) caused by interaction between the upcoming S wave and multiple sP_mP (sP_mP) reflections in the crust (Langston, 1996). The s -PL train is developed efficiently at regional distances by deep earthquakes from upward radiated S wave impinging on continental crust (Furumura & Kennett, 2017; Kennett & Furumura, 2019). The record section in Figure 3 (out to 1,250 s) is terminated by the late arrival of high-frequency ScS phase that tends to merge with sS at larger distances, with lower frequency $sScS$ even later.

2.2. PGV Attenuation Function for the Very Deep Earthquake

The distribution of the peak ground velocity (PGV) for horizontal motion obtained from the Hi-net and F-net records for the 2013 Sea of Okhotsk earthquake is shown in Figure 5a. Large ground motion is observed on the Sea of Japan side of northern Japan from Hokkaido to Honshu, over 5 times as large as at the same distance on the Pacific Ocean side. This pattern corresponds well with the distribution of shaking intensity

shown in Figure 1a. The larger ground motion on the back-arc side of the Pacific slab subduction contrasts with the normal situation for events in Pacific slab (Figures 1b and 1c). The contrast is even more distinct in displacement (see Figure S1c in the Supporting Information), as this peculiar ground motion pattern is produced by low-frequency (<1 Hz) waves from the large, distant earthquake.

The attenuation of the PGV for horizontal and vertical motions as a function of epicentral distance is shown in Figure 5b. Relatively large fluctuations of about 0.5–2 times the PGV at similar epicentral distances occur due to the contrast in ground motion between the Pacific Ocean side (larger) and the Sea of Japan side (weaker) and some modest site amplification effects at the Hi-net and F-net stations. The plot of PGV versus epicentral distance shows anomalous amplification of ground motion in both horizontal and vertical motions, with a large peak in PGV near 2,000-km epicentral distance, and a gentle PGV bump around 2,400 km. With increasing epicentral distances (>2,800 km), the PGV of horizontal motion increases again to produce a third peak, but not for vertical motion. As we can see in the record section (Figure 3), the group of PGV maxima at certain distances is produced by a range of wave propagation phenomena.

At shorter distances (<1,500 km) strong PGV is associated with the arrival of the upward traveling *S* wave. The second peak (2,000 km) links to the interaction of upgoing waves from the deep source and downgoing waves that also interact with the 660-km discontinuity; there is also a gentle bump (2,400 km) due to sP. The third peak (>2,800 km) is associated with the arrival of the sS reflection. Near-vertical incidence of ScS from the core-to-mantle boundary may also increase the PGV for horizontal motion at larger distances.

Such peculiar PGV amplification and attenuation patterns are also seen for other earthquakes: (1) near the 2013 Sea of Okhotsk earthquake at a similar source depth, (5 June 2008; M_w 7.7; 610 km) and (2) a somewhat shallower earthquake (24 November 2008; M_w 7.3, 500 km; see, Figure S2 in the Supporting Information). Thus, the results from the 2013 Sea of Okhotsk earthquake can be considered to be a common feature for all deep events in this locality, which lies quite far from the Japanese islands.

2.3. Three-Component Records

To provide more detail of the properties of the ground motions that induce larger PGV at certain distance in Japanese islands, we show in Figure 6 the three-component records of F-net stations at epicentral distance of (a) 1,374 km (NKGf), (b) 1,921 km (GJMF), (c) 2,458 km (KNMF), and (d) 3,171 km (TASF).

The records for the largest PGV in northern Hokkaido (NKGf; Figure 6a) indicate that the large-amplitude, short-duration *S* phase is formed by upward radiating *S* wave from the deep (610 km) source that travels to stations across the Sea of Okhotsk.

The second group of large PGV at Tohoku near Akita (GJMF; Figure 6b) is linked to a large and rather complicated wave packet caused by near caustics of the *S* wavefront associated with the triplication of upgoing and downgoing waves from the deep source and refracted/reflected waves from the 660-km discontinuity. The *S* wave also shows sP precursor of *S* and sPmP reflections after *S* on the *R* and *Z* components.

The waveform at KNMF (Figure 6c) at distance of 2,458 km, where a weak bump in PGV was observed, shows a distinct sP conversion on the *R* and *Z* components with amplitude as large as *S* on the *Z* component. On the *T* component, the core reflected ScS phase produces the maximum ground motion. Thus, the large PGV around this distance is explained by large sP and ScS phases. The particle motion of the long-period ground motions following *S* shows prograde motion in *R*-*Z* plane with weakly dispersed features, indicating the s-PL wave generated by the coupling between the upcoming *S* and sPmP reflections traversing the crustal waveguide (see Figure S3 in the Supporting Information). Such coupling in the crust also occurs for sS (sS-PL) to make long *S* wave trains.

In the three-component records for much larger distance (3,171 km, TASF, Figure 6d), we see a large sS reflection and ScS core reflection on the *T* component, with amplitude much larger than *S*. These large phases explain the increase in PGV at large distances greater than 2,800 km (Figure 5b). At such distances the upcoming *S* wave to the free surface goes post critical to make large sS and weak sP.

3. Simulation of Ground Motions for the 2013 Sea of Okhotsk Earthquake

We gain further insight into the nature of the propagation processes that control the ground motion pattern for the very deep 2013 Sea of Okhotsk earthquake, by conducting 3-D FDM simulations with comparison to the observations from the dense Hi-net and F-net stations across Japan.

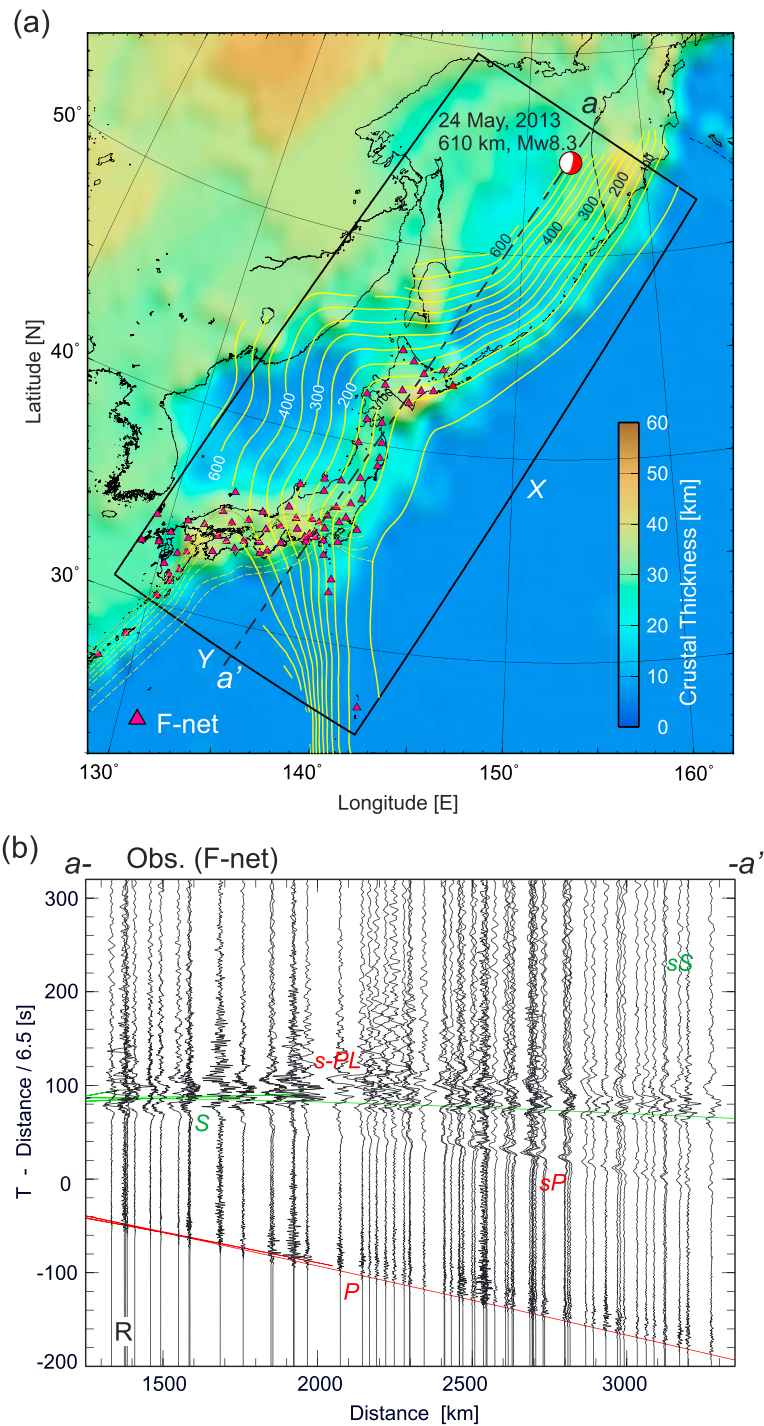


Figure 7. (a) Model used for 3-D FDM simulation of seismic wave propagation illustrating the area of simulation and configuration of Pacific and Philippine sea slabs, and the thickness of the crust (from CRUST1.0). Locations of the F-net stations are shown in purple triangles. (b) Observed record section of *R* component ground velocity recorded at the F-net stations inside the simulation domain.

3.1. Simulation Model

The volume used for the 3-D FDM simulation is 3,360 km by 1,536 km in the horizontal direction and 1,200 km in depth. The model covers the area from the south of Kamchatka to Kyushu, discretized with a grid interval of 0.5 km in horizontal direction and 0.25 km in vertical (Figures 7a and 8). Core phases are not

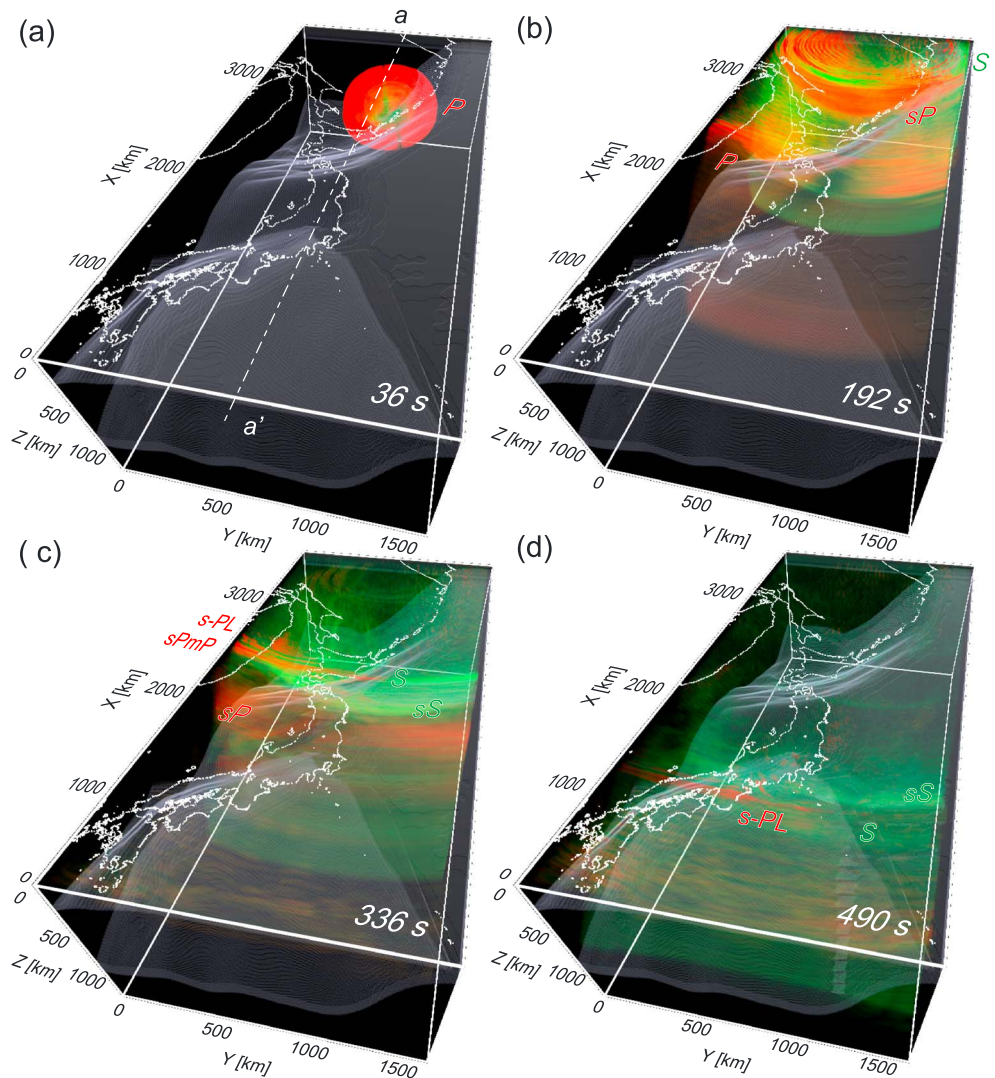


Figure 8. Snapshots of 3-D seismic wavefield for the 2013 Sea of Okhotsk earthquake derived by the simulation using a point double-couple source, displaying the *P* and *S* wavefield in red and green, respectively, at 36, 192, 336, and 490 s after earthquake initiation. Also see Movie S2.

considered in this simulation. The FDM simulation was performed in a Cartesian coordinate system using the OpenSWPC code (Maeda et al., 2017). Earth flattening is applied to compensate for the sphericity of the Earth.

Stochastic random heterogeneities in the crustal structure are implemented by using a von Karman distribution function with correlation distance of 10 km horizontally and 0.5 km vertically, with a standard deviation of 2%. For mantle structure, we impose similar heterogeneity with correlation distances of 10 km horizontally and 5 km vertically and a standard deviation of 1%. These perturbations are superimposed on the background velocity and density. Such small-scale heterogeneity is necessary to simulate the scattering and guiding of high-frequency ($f > 1\text{--}2$ Hz) signals, the effect is less important for the low-frequency (< 1 Hz) wavefield with much longer wavelength than the dominant scale of heterogeneity.

With the minimum wave speed of $V_p = 1.5$ km/s, in seawater, in the simulation model and the need for sampling of 5 grid points per minimum wavelength, the simulation is suitable for wave propagation up to a frequency of 0.6 Hz (Nyquist frequency 1.5 Hz). The 3-D simulation requires 22.8 Tb of computer memory in single-precision calculations and wall clock time of 8.9 hr for modeling wave propagation to 900 s with 100,000 time steps ($\Delta t = 0.009$ s) using 2,106 nodes of the Earth Simulator supercomputer at the Japan Agency for Marine-Earth Science and Technology.

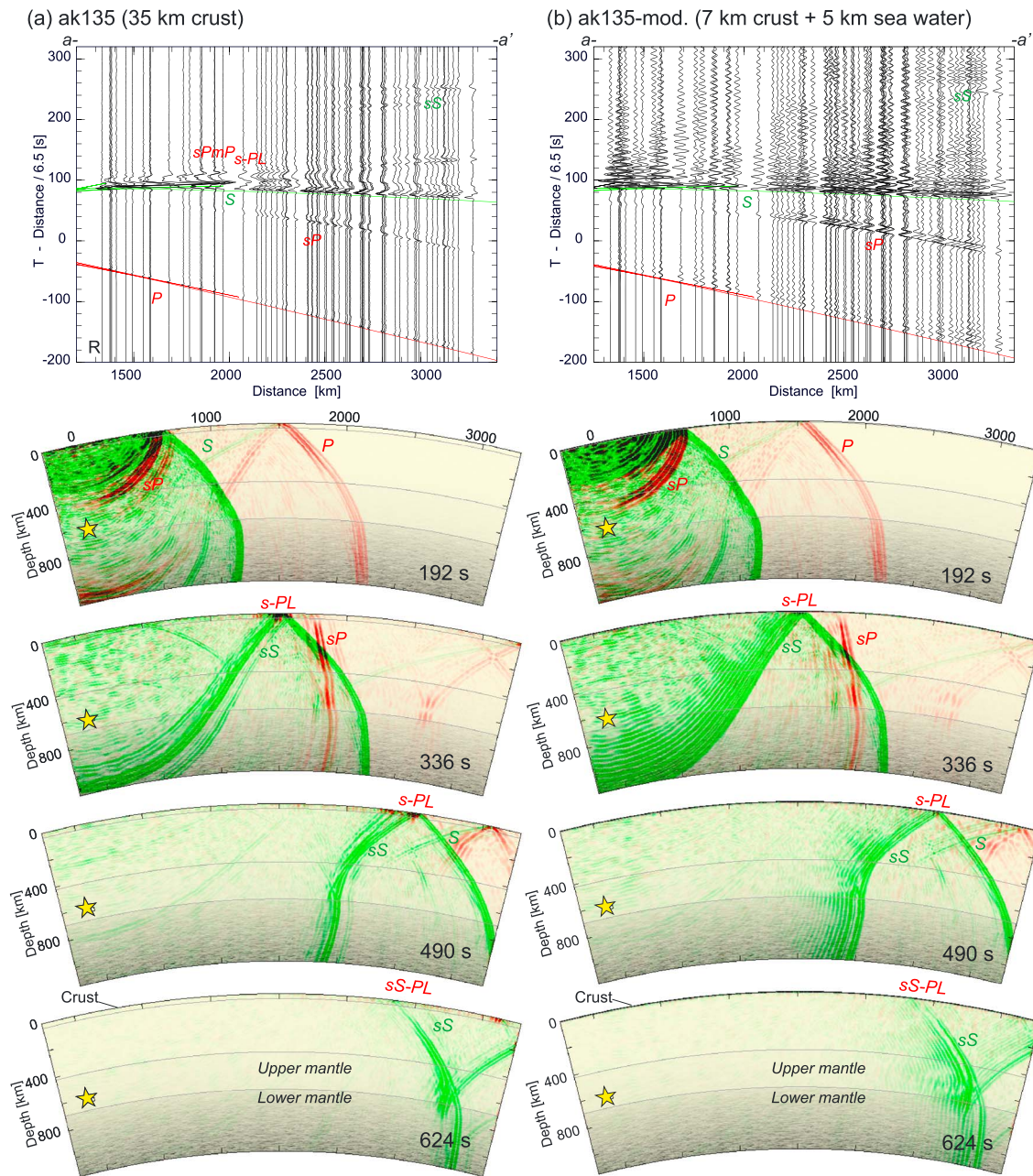


Figure 9. Snapshots of seismic wave propagation at 192, 336, 490, and 624 s after the earthquake initiation, together with a synthetic record section of R component ground velocity at F-net stations (see Figure 7a for locations) obtained by 3-D FDM simulation using (a) the ak135 standard Earth model (35-km thick crust) and (b) modified model with 7-km crust and 5-km-thick seawater and receivers at the seabed. Major phases are marked.

3.1.1. Simulation for Thick Crust

We first examine the wavefield for a simple crust and mantle structural model using the ak135 standard earth model (Kennett et al., 1995) with a 35-km-thick continental crust. The anelastic (Q_p and Q_s) structure of Montagner and Kennett (1996) is employed to introduce attenuation. A double-couple point source is placed at 610-km depth using the Global Centroid-Moment-Tensor (GCMT) moment tensor solution (strike = 189°, dip = 11°, rake = -93°), with a source-time function of an 8-s triangle.

The results of the simulation for the laterally homogeneous 35-km-thick crust model are shown in Figure 9a with snapshots of seismic wave propagation at 192, 336, 480, and 624 s from earthquake initiation, along a vertical profile across source to Kyushu though Hokkaido and Honshu (a--a' in Figure 7a). The simulated

wavefield is separated into P and S waves by taking the divergence and curl of the 3-D wavefield. P waves are shown in red and S waves in green. The record section of R component ground velocity for the F-net stations is shown with a reduction velocity at crustal P wave speed (6.5 km/s). Each trace in the record section is multiplied by epicentral distance to compensate for the geometrical attenuation of body waves.

The first frame of the snapshot (192 s) displays upgoing P and S waves from the deep (610 km) source, producing a triplication of the S wavefront with upward and downward radiating waves from the source and reflected waves from the 660-km discontinuity. This makes a large amplitude near-caustic S phase at epicentral distance around 1,500 km. The incidence of the S wave at nearly critical angle to the free surface at distances over 600 km produces strong sP conversion, which then travels in the crustal waveguide by wide angle PmP reflections (sPmP) and by sPn in the mantle (336-s snapshot). These crustally guided sPmP phases interfere with the upcoming S wave, giving rise to a long-period s-PL wave partially trapped in the crust (336- and 490-s snapshots). Usually, the attenuation of s-PL is significant, as conversion to S at the free surface extracts P wave energy from the crustal waveguide by leakage into the mantle, but s-PL from deeper earthquakes can sustain ground motion for rather long distances (>1,000 km) as continuously upcoming S wave from the deep source compensate for the loss (Furumura & Kennett, 2017).

As the epicentral distance increases, the incident angle of upcoming S wave to the crust becomes post critical, and a totally reflected sS wave into the mantle travels to larger distances beyond about 3,000 km (624-s snapshot). This also produces a long-period sS-PL wave train. The record section shows large, impulsive S waves at shorter distances (<2,000 km), that switch at larger distances to lengthy wave trains formed by sP, S , and s-PL waves lasting several minutes.

3.1.2. Simulation for Thinner Crust

To look at the effect of the near-surface conditions, we also conduct a FDM simulation using a modified version of the ak135 model with 7-km-thick crust and a 5-km seawater on the top. The receiver is placed at the seafloor.

The result is shown in Figure 9b, where very long and monochromatic P and S wave codas are a prominent feature due to multiple reverberations in the thinner crust and seawater. Such features can be found in the observed records shown in Figure 6 traveling across the Sea of Okhotsk and Sea of Japan, though the simulation results have much stronger reverberations due to a large impedance contrast between seawater and upper crust.

The sP reflection from thinner (7 km) crust is much stronger than for thicker crust (192-s snapshot) even for shorter epicentral distances. However, the thinner crust cannot sustain sPmP reflections within the crust for large distances, and the generation of s-PL is very weak (336- and 480-s snapshots). As a result of large S to P conversion at the free surface, the sS reflection becomes weaker (490- and 624-s snapshots).

When compared with the record section for the thicker (35 km) crust model (Figure 9a), the wave propagation in the thinner crust shows strong sP for large distances, with amplitude, is as large or larger than S at epicentral distances over 2,400 km. On the other hand, sS reflection from the thinner crust is very weak and is almost concealed by long S reverberations.

The results of the simulations confirm that the strength of sP and sS arrivals from deep earthquakes are strongly influenced by the crustal structure around the reflection zone for the upcoming S wave; thick continental crust produces weak sP and strong sS, with the opposite effect for thinner oceanic crust. In S4 and S5 of the Supporting Information, we compare the strength of sP and sS with the crustal structure around the reflection points for the observed F-net and IRIS records, and ocean bottom broadband records on the North Pacific Ocean for the 2013 Sea of Okhotsk earthquake.

3.2. Wave Propagation in Heterogeneous Crust and Mantle Structure

For the full model of the 3-D FDM simulation we include realistic crust and mantle structures, and both the subducting Pacific and Philippine Sea slabs. We use this model to understand the features of the observed wavefield during the 2013 Sea of Okhotsk earthquake. In particular, we examine the effect of the subducting Pacific slab on the observed regional seismic wavefield by comparing the model with and without the slab.

3.2.1. Simulation Results With Laterally Varying Crustal Structure

The first stage is to include variations in the crust. We use the CRUST 1.0 model (Laske et al., 2013), which has a maximum crustal thickness of 38 km along the backbone of the Japanese islands, with gradually

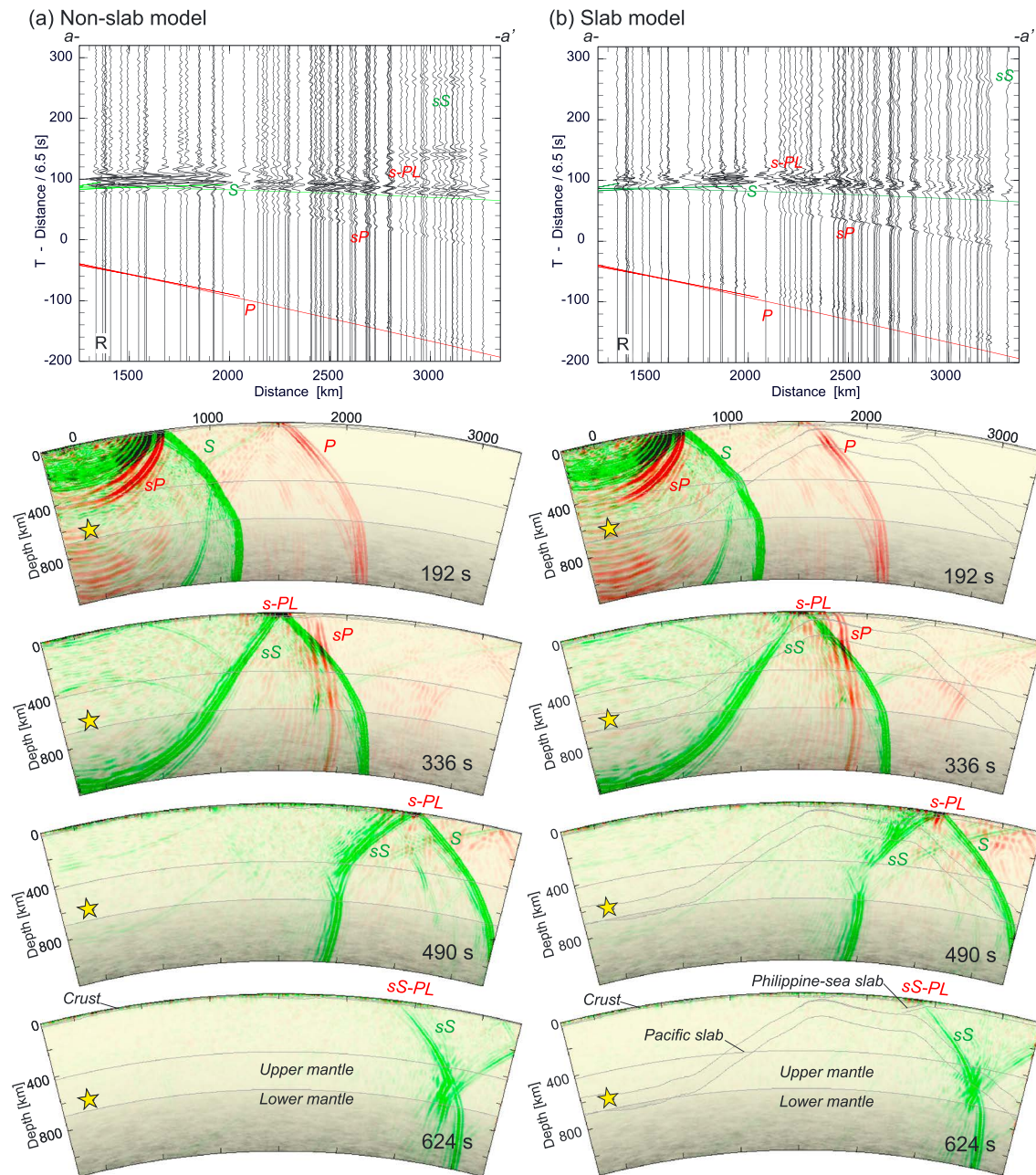


Figure 10. Synthetic record section of R component ground velocity for F-net stations (see Figure 7a for locations) and snapshots of seismic wave propagation at 192, 336, 490, and 624 s from the earthquake initiation, along vertical profile a--a' (see Figure 7a), obtained from the 3-D FDM simulation using (a) laterally heterogeneous crustal model (from CRUST1.0) and (b) with subducting Pacific and Philippine Sea slabs. Also see Movie S3.

thinning crustal thickness toward the Pacific Ocean and the Sea of Japan to connect to oceanic crust about 7 km thick (Figure 7a). We applied the same stochastic random heterogeneities in the crust and mantle as used in the simulation with the simple model shown in Figure 9.

In this simulation we use a finite source-rupture model for the 2013 Sea of Okhotsk earthquake obtained by an inversion of teleseismic waveforms (Wei et al., 2013), described by four subevents over a 140-km \times 50-km fault plane; the rupture runs at an average speed of 4.0 km/s and radiates seismic wave with total seismic moment of 4.8×10^{28} dyn cm. This source model is described by 391 double-couple point sources over the fault plane. This simulation does not include any subducted slabs.

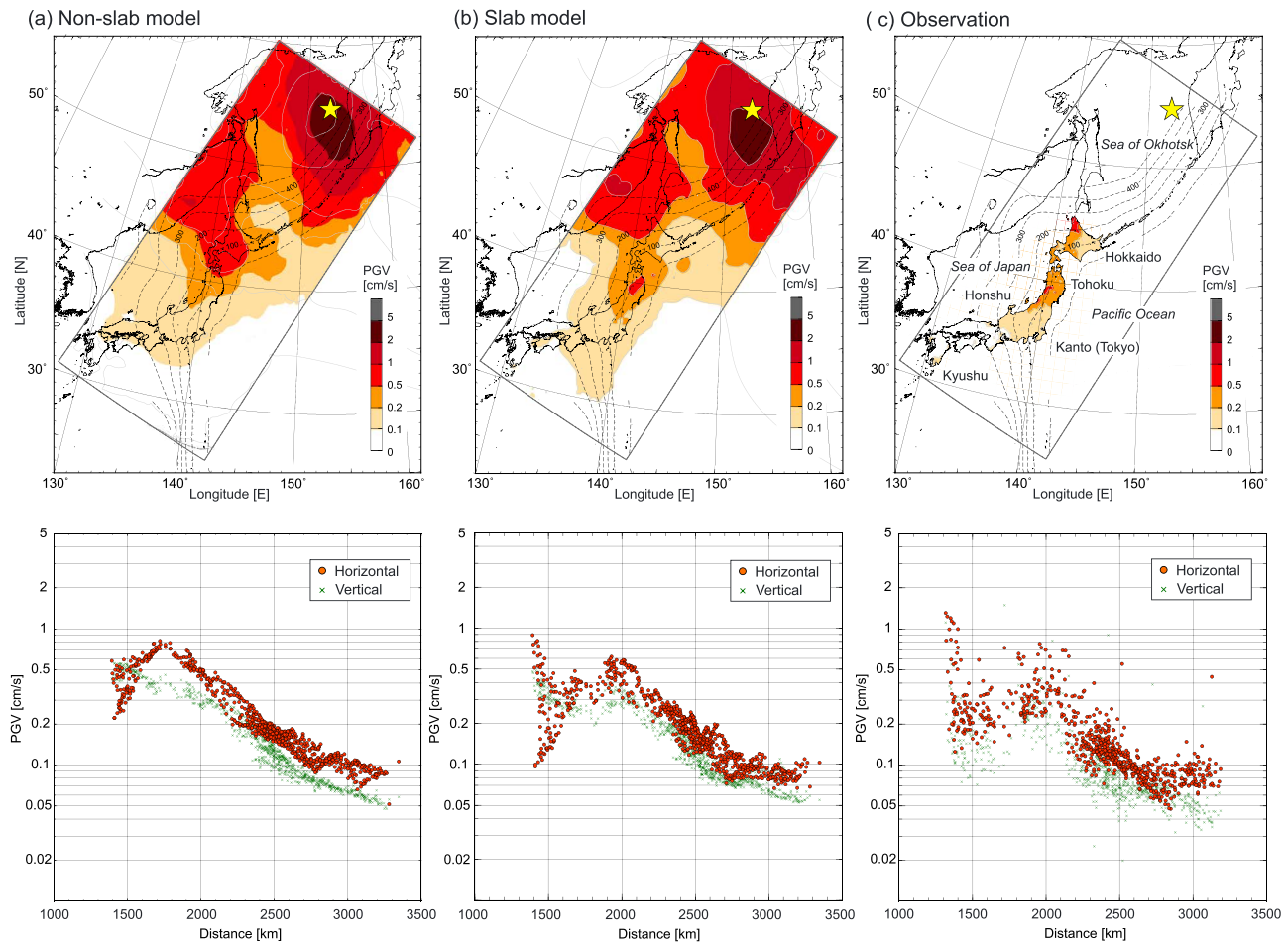


Figure 11. Comparison of the simulated PGV and attenuation function of the PGV for horizontal (orange circles) and vertical (green crosses) as a function of epicentral distance obtained by the 3-D FDM simulation using (a) the CRUST1.0 model (Figure 10a) and (b) CRUST1.0 and Pacific slab (Figure 10b), to examine the effect of subducting slabs. (c) Observed PGV pattern from the Hi-net and F-net stations and attenuation function (repeat of Figure 5).

The result of the crustal simulation with the finite source-rupture model for snapshots of the seismic wavefield and the record section of *R* component ground motion are shown in Figure 10a. The snapshots are shown for the FDM results using a point double-couple source with an 8-s triangular time function to increase the visibility of the phases and allow comparison with the simple layer models. In Figure S6 of the Supporting Information, we compare simulations with the simple point source for both the simple structure and the model derived from CRUST 1.0 to examine the influence of larger-scale variability in crustal structure on the seismic wavefield.

The long and incoherent *P* and *S* wave codas developed by traveling through heterogeneous crust agree well with the observed ground motion from the M_w 8.3 earthquake displayed in Figure 7b. There are large variations in the strength of sP and sS and wave shape of s-PL wave among traces as they traverse the laterally varying crustal waveguide (Figure 10a).

The distribution of PGV across the Japanese islands and the attenuation function of PGV obtained from the FDM simulation at the location of F-net and Hi-net stations are shown in Figure 11a, which is to be compared with the observation from the 2013 Sea of Okhotsk earthquake (Figure 11c). The simulated PGV map shows north-south stretched PGV contours above the source due to the *S* radiation pattern and the source-rupture effect and further large distortions due to variation in crust and mantle structure. In this model without subducted slabs, a band of larger (>0.5 cm/s) PGV lies across the center of Hokkaido at epicentral distance about 1,700 km. This enhanced ground motion is due to the arrival of the near-caustic *S* triplication and lies much closer to the source than in the real scenario (around 2,000 km).

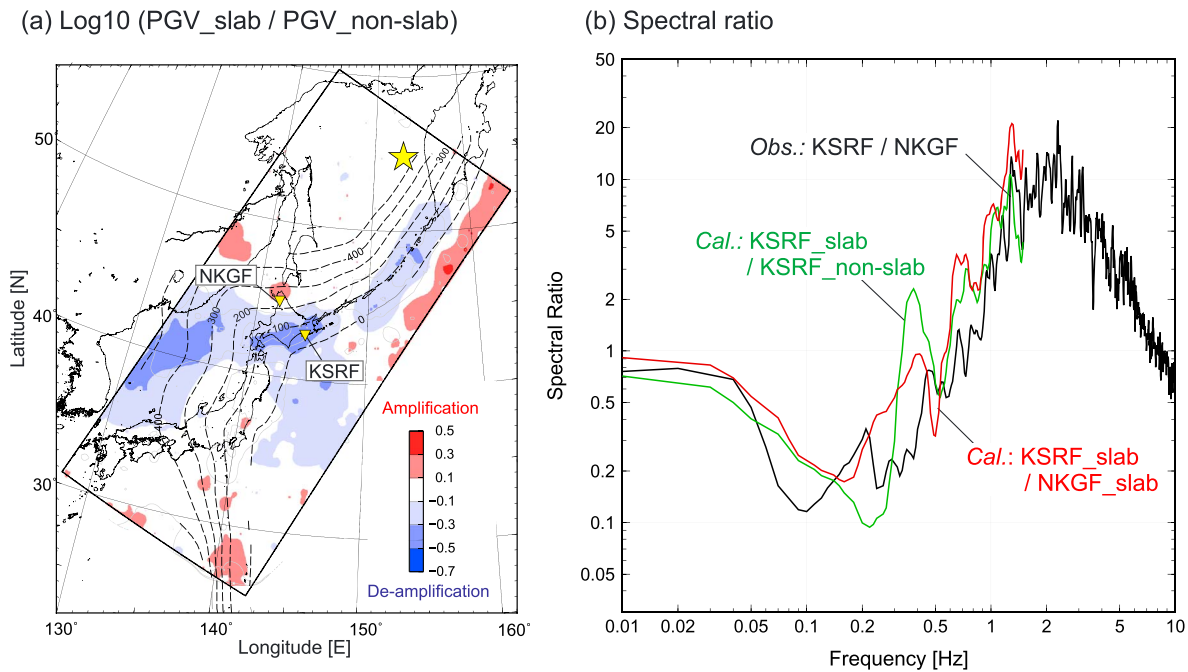


Figure 12. (a) Ratio of PGV obtained by the 3-D FDM simulation with and without the slab; blue and red denote the area of de-amplification and amplification of the PGV due to the Pacific slab, respectively, shown in logarithmic scale. (b) The spectral ratio for the *S* wave at station KSRF of the slab model relative to the non-slab model (green line), and the spectral ratio of *S* wave at KSRF to that of a reference station (NKGF; KSRF/NKGF; red line), comparing with the spectral ratio of observed ground motions (KSRF/NKGF; black line).

3.2.2. Simulation Result With Subducting Slabs

We now complete the model by including the 3-D configuration of the subducting slabs and examine the way in which the Pacific plate modifies the regional wavefield from the 2013 Sea of Okhotsk earthquake.

The depth to the Pacific slab is based on the work of Yokota et al. (2017), assuming a plate thickness of 100 km and a 7-km oceanic crust at the top. The depth of the Philippine Sea Plate is obtained from the JIVSM (Koketsu et al., 2008) with a plate thickness of 30 km and an oceanic crust thickness of 7 km. However, the effect of the Philippine Sea slab in the west of Japan is likely to have little effect for this large earthquake in the Pacific slab. The distribution of velocity and stochastic random heterogeneities in the oceanic crust and lithosphere of the subducting slabs are taken from Kennett and Furumura (2015).

The result of the 3-D FDM simulation with both laterally varying crust and subducting slabs is shown in Figure 10b, with a 3-D visualization of the seismic wavefield shown in Figure 8 and Movie S2. The distribution of the PGV and the corresponding attenuation function for this simulation with slabs are displayed in Figure 11b. The snapshots of the seismic wavefield show an upward bend in the *S* wavefront as it traverses the high-wave speed slab (192-s snapshot). This increases the incident angle of the *S* wave to the free surface to develop larger sP at shorter distances (192- and 336-s snapshots). The sP phases then travels longer distances in the mantle as sPn to generate large ground motion around 2,400-km epicentral distances and in the crust as multiple sPmP reflections to lead s-PL (490-s snapshots).

The simulated record section shown in Figure 10b demonstrates the significance of sP phases over a large distance range across Japan from Hokkaido to Kyushu. Compared with the record section without the presence of the slabs (Figure 10a), the ground motion at shorter distances (<2,000 km) decreases as the radiation pattern of the *S* wave is modified after traversing the high-wave speed slab. The duration of the long-period *P* and *S* codas are much enhanced by interaction with the 3-D heterogeneous structure in the subducting slabs. The synthetic record section (Figure 10b) is consistent with the features seen in the observed waveform at F-net stations (Figure 7b).

The result of the PGV distribution across Japan with the Pacific slab (Figure 11b) is greatly modified from the situation without a slab (Figure 11a). The areas of larger ground motions spread to north and south around the 100-km isodepth marker for the Pacific slab. This explains the peculiar PGV and intensity pattern caused

by the 2013 Sea of Okhotsk earthquake (Figure 11c, also see Figures 1a and 5a), with a separation of intense ground motions in northern Hokkaido and in Tohoku at the Sea of Japan side. The modification of the ground shaking occurs due to the bending of the wavefronts for low-frequency (<1 Hz) seismic waves away from the high-wave speed slab. Such an antiwaveguide effect of a high-wave speed subducting slab is very efficient for low-frequency waves (Chen et al., 2007; Furumura & Kennett, 2008; Vidale, 1987) in contrast to the waveguide effect for high-frequency (>1 Hz) seismic waves as a result of strong forward scattering in heterogeneous slab (Furumura & Kennett, 2005). Thus, for large and distant earthquakes with dominance of low-frequency signals, the antiwaveguide process can be expected to override the high-frequency waveguiding. This combination produces the peculiar PGV distribution of the 2013 Sea of Okhotsk earthquake at regional distances.

The inclusion of the subducting slab changes the pattern of S propagation to be consistent with the observations and the attenuation function. The plot of the simulated PGV attenuation function (Figure 11b) reflects the observed drop of PGV in southern Hokkaido to Tohoku at distances between 1,500 and 1,800 km (Figure 11c), due to the antiwaveguide effect of the Pacific slab, resulting in a migration of large PGV to Tohoku at epicentral distance of about 2,000 km. The slight increase in the PGV at distance around 2,400 km is due to the arrival of large sP and that beyond 2,800 km to the arrival of sS .

3.2.3. Spectral Ratio

The antiwaveguide effect of the high-wave speed slab for lower frequencies is confirmed by the behavior of the map of the ratio of the PGV between models with (Figure 11b) and without the slab (Figure 11a), as shown in Figure 12a. The map of the ratio shows a band of weakened PGV parallel to the isodepth contour of the Pacific slab and increased PGV outside of the slab due to the refraction of seismic waves toward the low-wave speed mantle on the outside.

We consider the F-net stations NKGf and KSRF (see Figure 12a for location). The spectral ratio of the synthetic S waveform at KSRF for models with and without the slab displays a significant deamplification of ground motions by $1/2$ – $1/3$ in the frequency range between 0.04 and 0.3 Hz (3 to 25 s; Figure 12b, green line). Similar deamplification for low frequencies due to the slab antiwaveguide effect can be confirmed by comparison between the spectrum of S wave at KSRF relative to the reference station NKGf (Figure 12b, red line), which is consistent with the observed ground motions (Figure 12c, gray line). Such slab antiwaveguide effect is important in this frequency range, but not at very low frequencies because the wavelength is then too long to be captured by a thinner slab (Furumura & Kennett, 2008).

The spectral ratio results also show a waveguide effect for high-frequency waves (>0.5 –1 Hz) with increase in the spectral ratio of the S wave to 10–20 with increasing frequency to 3 Hz (Figures 12b). However, in the case of large, distant earthquakes, low-frequency (<1 Hz) wavefields become dominant at regional to teleseismic distances and control the observed PGV and intensity patterns. In PGA, where high frequency is intensified, we can see some effect of the slab waveguide effect to cause larger shaking on the Pacific Ocean side (Figure S1a), similar to the intensity patterns of nearby earthquakes (Figures 1b and 1c).

4. Teleseismic Ground Motion Observations

Not only did the 2013 Sea of Okhotsk earthquake produce complex, long-duration ground motion across the Japanese islands associated with the S , sP , and $s-PL$ waves, but the sS wave reflected by the thick crust of the Japanese archipelago traveled several thousand kilometers through the mantle to be felt at teleseismic distances. In this section we examine the propagation of long-period ground motion to teleseismic distances by multiple reflections at free surface and the cause of reported felt ground motion at extraordinarily large distances.

4.1. Felt Reports at Teleseismic Distances

According to the USGS's Did you feel it? (USGS, 2013), felt reports equivalent to MMI 4 to 6 were posted in Dubai, northern India, and California, etc., at large epicentral distances, greater than 6,000 km (Figures 13a and 13b). According to newspaper reports, people in Moscow, 7,379 km away, were evacuated from upper floor of high-rise buildings due to large and uncomfortably long duration of shaking (Earthquake-Reports.com, 2013; RT, 2013). Also, many city residents felt swaying of buildings at the top floors of high-rise buildings of 7–10 floors at Atyrau, western Kazakhstan 7,196 km away (Ak Zhaiyk, 2013).

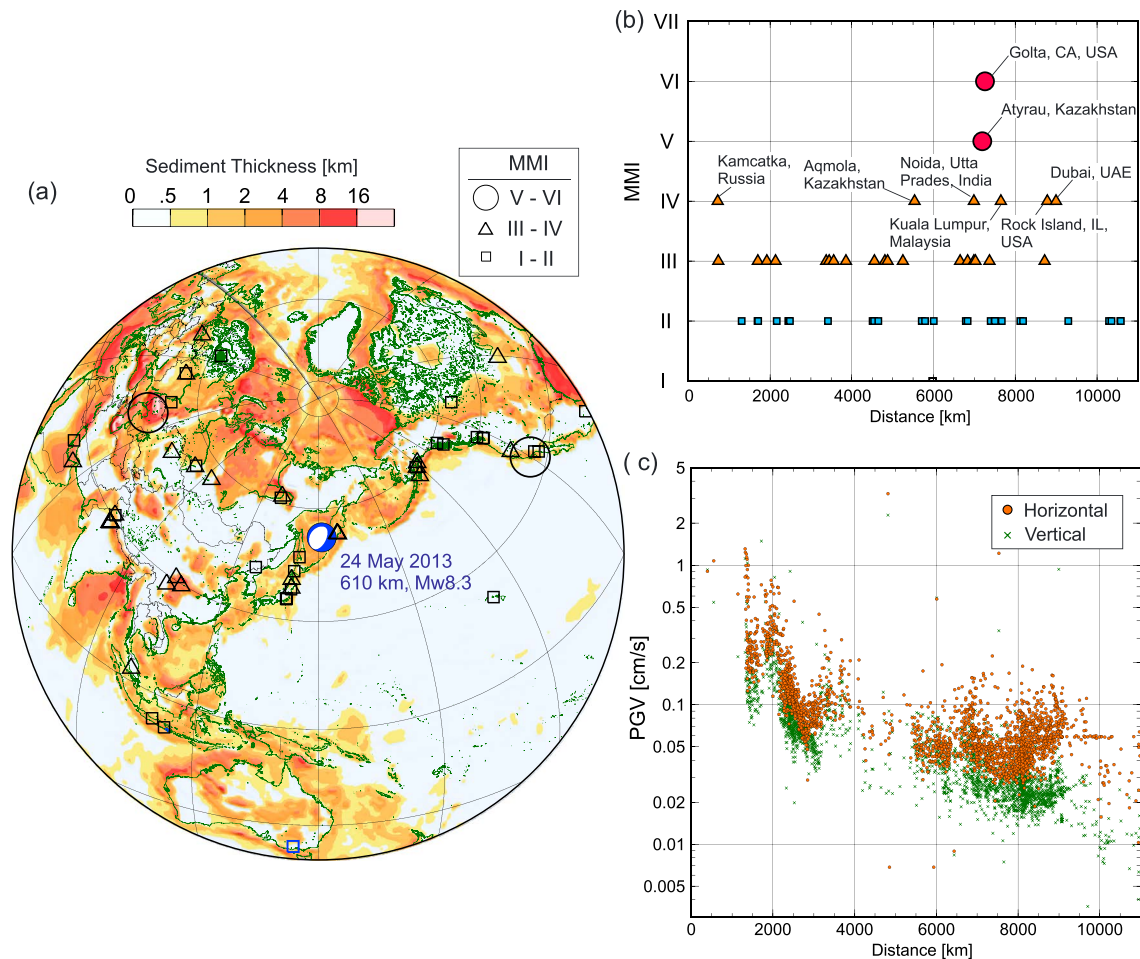


Figure 13. (a) Map showing the location of the felt report (after USGS Did you feel it?, USGS, 2013) on the map showing the thickness of sedimentary layer from CRUST1.0. (b) Plots of felt report as a function of epicentral distance and value of report equivalent to MMI. (c) Attenuation function of peak PGV of horizontal (orange circles) and vertical (green crosses) motions as a function of epicentral distance obtained by F-net, Hi-net, and IRIS DMC data.

Such large and lengthy shaking of tall buildings reminds us of long-period (2–10 s) ground motions amplified by thick sedimentary basins during large earthquakes (e.g., Chen et al., 2018; Cruz-Atienza et al., 2016; Denolle et al., 2014; Furumura & Hayakawa, 2007; Koketsu et al., 2005). The distant felt reports for the 2013 Sea of Okhotsk earthquake are concentrated in population centers, commonly situated on thick sedimentary basins, at epicentral distances of 5,000–8,000 km (Figure 13b).

Similar felt reports at large distances from very deep earthquakes were made for the 1994 Bolivia earthquake (depth = 637 km, M_w 8.3), and many of the felt reports come from upper floors of multistory buildings indicating relatively low frequency ground motions compared with large, high-frequency ground acceleration of nearby earthquakes (Anderson et al., 1995; Frohlich, 2006). Anderson et al. (1995) examined the teleseismic records for this earthquake and claimed that the shaking in North America as far as 8,680 km from the epicenter was associated with P and PcP waves, linked to the radiation pattern of the source, high- Q of lithosphere, site, and structural amplification effect. Following this study, Kuge (2015) analyzed IRIS DMC broadband data for the 2013 Sea of Okhotsk earthquake and confirmed that once again, the observed ground motions at teleseismic distances are in correspondence with the radiation pattern of the P wave and the high- Q structure of the lithosphere.

With the understanding we have gained of the regional wavefield across Japanese islands, we re-examine the propagation properties of seismic waves for the 2013 Sea of Okhotsk earthquake out to teleseismic distances, combining observations from F-net, Hi-net, and the IRIS DMC for 1,854 stations for epicentral distances up to 12,000 km (Figure 13c). The attenuation function for PGV for horizontal motion from regional to

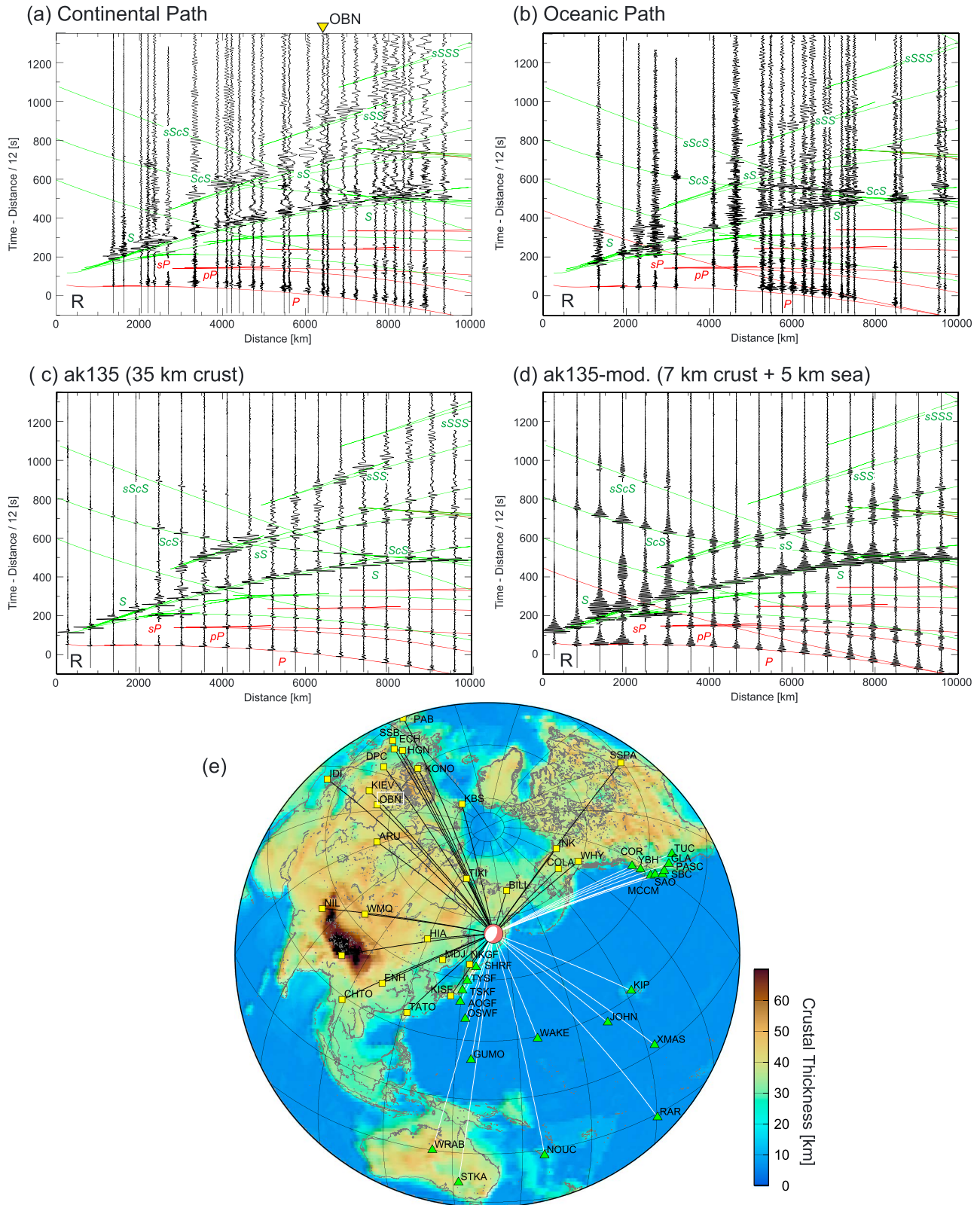


Figure 14. Record sections of R-component ground velocity illustrating for IRIS stations along (a) continental path (black lines on the map) and (b) oceanic path (white lines on the map). (c) Synthetic record section obtained by the FDM simulation using (c) the ak135 standard Earth model (35-km-thick crust), and (d) a modified model for oceanic structure (7-km-thick crust and 5-km-thick seawater). (e) Map showing the crustal thickness and raypaths from source to stations.

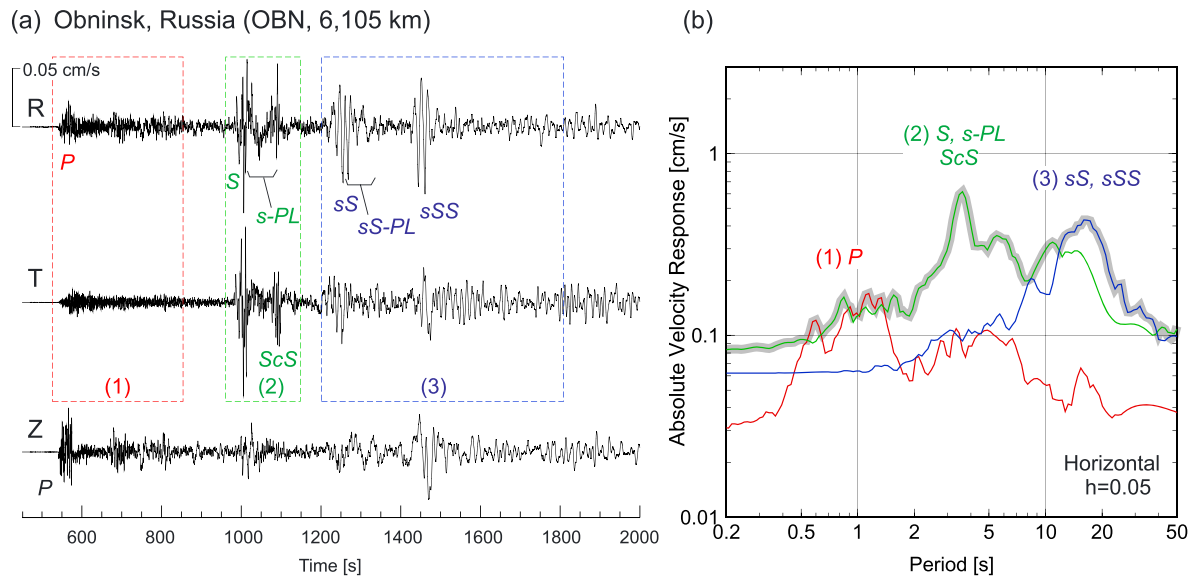


Figure 15. (a) Three-component ground velocity records obtained at Obninsk Russia (OBN) at epicentral distance of 6,105 km. (b) Absolute velocity response spectrum of horizontal motions obtained by whole waveform (gray line), (1) *P* wave (red line), (2) *S* and *ScS* phases (green line), and (3) *sS* and *sSS* phases (blue line). Time window of each phase is shown in the record section.

teleseismic distances tends to increase beyond 2,800 km and has a peak at far-regional distance of about 4,000 km, which is explained by *sS* reflections as we have seen in the F-net records in Japan (Figures 3 and 5b). There are noticeable fluctuations in the PGV pattern but indications of a further peak in the horizontal motion at epicentral distances around 7,000–9,000 km due to the arrival of *sSS*. The shaking reports at larger distances (5,000–8,000 km; Figure 13a) during the 2013 Sea of Okhotsk earthquake correspond to the zone with elevated PGV in the horizontal component of broadband records (Figure 13c).

4.2. Long-Period *S* Reflections From Thick Continental Crust

In the Did you feel it? (USGS, 2013) a single felt report for the 2013 Sea of Okhotsk came from the island of Hawaii; the rest were from major population centers on the continents, which are commonly situated on thick sedimentary basins (Figure 13a).

The record section of *R* component ground velocity for the IRIS stations out to 10,000 km from the epicenter along continental paths (Figure 14a) shows lengthy long-period (>3 s) ground motions at distance around 4,000 km that can be linked to *sS* and *sS-PL*, and near 8,000 km corresponding to the double bounce *sSS* and *sSS-PL*. The general behavior is well reproduced with a 2-D FDM simulation using a point source with a 10-s triangular signature in the ak135 standard Earth model with a 35-km-thick crust (Figure 14c). To eliminate effects from radiation patterns, a combination of an explosion and a torque source was employed in this simulation. Felt reports from cities on the continents are therefore likely to be caused by such long-duration shaking of long-period ground motions from the multiply reflected *S* waves.

Such long-period ground motions are not evident at stations in an oceanic environment (Figure 14b), because the thin oceanic crust does not produce large *sS*, as is confirmed by FDM simulation with an oceanic crust model (Figure 14d). Instead, the record section at teleseismic distances is characterized by long reverberations of relatively high frequency *P* and *S* body waves and the *ScS* phase in the oceanic structure (Figures 14b and 14d).

4.3. Effect of Long-Period Ground Motions for Distant Felt Reports

Figure 15a shows the three-component ground velocity records at Obninsk (OBN, 6,105 km; see Figure 14e for location), near Moscow where the 2013 Sea of Okhotsk earthquake was reported to be felt. The three-component records show large *sS* and *sSS* reflections following *S*. Long-period ground motions last over a dozen minutes including contributions from the *s-PL*, *sS-PL*, and *sSS-PL* wave trains.

The absolute velocity response spectrum for horizontal ground motion at OBN shows a maximum velocity response of 0.6 cm/s at a period of 3.5 s (assuming a 5% damping), and relatively large (>0.3 cm/s) response

continues in the longer-period band up to 20-s period (Figure 15b). From the response spectrum in the time window of each phase, we see that the long-period response is associated with S and ScS waves up to 6-s period and then by sS and sSS waves for longer periods. The response of P wave is small (<0.2 cm/s) and in a much shorter period band (<1.5 s).

Japan Meteorological Agency defines a second intensity scale (max 4) for long-period (3–10 s) ground motion, in addition to the traditional shaking intensity (max 7) for short-period ground motion (around 0.5–1 s). This second intensity scale is based on the absolute velocity response spectrum in the period range 3–10 s and is used to assess the effect on the shaking of high-rise buildings. The calculated velocity response at OBN is less than the lowest level, but it could rise to rank 1 (>5 cm/s) if several fold amplification occurred from the effect of a sedimentary basin. Rank 1 corresponds to the situation that most people in a high-rise building feel swaying, and hanging materials such as blinds shake strongly.

Such sedimentary amplification for long-period ground motion is likely to be the reason that people felt shaking in high-rise buildings in Russia and Kazakhstan from the 2013 Sea of Okhotsk earthquake, due to the resonance with long duration of long-period ground motions lasting up to 10 min—with efficient propagation of S multiples on the continental path, in addition to high-frequency P wave.

5. Conclusions

Strong ground motion from large and very deep earthquake as for the 2013 Sea of Okhotsk earthquake (610 km, M_w 8.3) extends over large areas, even to teleseismic distances. We have been able to unravel the complex nature of the wavefield caused by the earthquake from regional to teleseismic distances by utilizing the dense Hi-net array, F-net records, and IRIS DMC data, complemented by 3-D FDM simulations of seismic wave propagation.

The directly visualized seismic wavefield from the dense seismic records, and high-resolution FDM simulations using detailed structure of the Pacific plate subduction zone, demonstrates the way in which crust and subducting slab contribute to the wavefield from very deep earthquakes very dramatically. Surface reflection of upgoing S waves to develop sP and linked $s-PL$ produce lengthy wave trains at shorter distance. Farther away from the source S is important and interacts with the full pattern of S waves both upgoing and downgoing from the source and reflections from the 600-km discontinuity, to sustain large long-period disturbances.

The results of the 3-D FDM simulation revealed the complex nature of the upgoing S wavefield from the very deep earthquake and are consistent with the character of the observations. However, some of the mismatch in detail between the observed waveforms and the synthetic seismograms are likely to be due to the relatively simple Pacific slab model employed in the simulation. As shown in Figure 11, the distribution and attenuation property of PGV over Japanese island is very sensitive to the slab structure. Thus, it should be possible to refine the slab model by comparison of observations and simulations. The frequency dependence of the waveguide and antiwaveguide effects from the subducting slab provides a means of further investigation of detailed structure inside the slab.

The S phase and its multiple reflections can carry energy to considerable distances along continental paths even to teleseismic distances, and the long-period effects can be reinforced by associated $sS-PL$, $sSS-PL$ phases partially trapped in the continental crust. With amplification by sedimentary basins and resonance of multistory buildings, there is potential for felt shaking from very deep earthquakes even at teleseismic distances.

References

- Ak Zhaiyk (2013). Atyrau shaken by earthquake (update). <https://azh.kz/en/news/view/1584>
- Anderson, J. G., Savage, M., & Quaaas, R. (1995). "Strong" ground motions in North America from the Bolivia earthquake of June 9, 1999 ($M_w = 8.3$). *Geophysical Research Letters*, 22(16), 2293–2296. <https://doi.org/10.1029/95GL01808>
- Chen, H., Tsai, V. C., & Niu, F. (2018). Observations and modeling of long-period ground-motion amplification across northeast China. *Geophysical Research Letters*, 45, 5968–5976. <https://doi.org/10.1029/2018GL078212>
- Chen, M., Tromp, J., Helmberger, D. V., & Kanamori, H. (2007). Waveform modelling of the slab beneath Japan. *Journal of Geophysical Research*, 112, B02305. <https://doi.org/10.1029/2006JB004394>
- Cruz-Atienza, V. M., Tago, J., Sanabria-Gomez, J. D., Chaljub, E., Etienne, V., Virieux, J., & Quintanar, L. (2016). Long duration of ground motion in the paradigmatic valley of Mexico. *Scientific Reports*, 6(1), 38,807. <https://doi.org/10.1038/srep38807>

Acknowledgments

The Hi-net and F-net records used in this study are available at the NIED Web page (<http://www.seis.bosai.go.jp>). The GDSN records are provided by the IRIS Data Centre (<http://ds.iris.edu/ds/nodes/dmc/>). The Japan Integrated Velocity Structural Model (JIVSM) is available at the Web page of the Headquarters for Earthquake Research Promotion, Japan (http://www.jishin.go.jp/evaluation/seismic_hazard_map/lpshm/12_choshuki_dat/). The Pacific Plate model was provided by the Cabinet Office, Japan. The finite-source rupture model is obtained from the database of the SRCMOD website (<http://equake-rc.info/SRCMOD/>). The felt reports are available from the Earthquake Hazards Program of USGS (<https://earthquake.usgs.gov/data/dyfi/>). The FDM simulation is conducted using the OpenSWPC seismic wave propagation simulation code, which is distributed at GitHub (<https://github.com/takuto-maeda/OpenSWPC>). Maps in the paper are drawn using the Generic Mapping Tools (Wessel & Smith, 1998; <http://gmt.soest.hawaii.edu/>). This study was conducted with support from Grants-in-Aid from the Japan Society of Promotion Sciences (17 K01322). The computations were conducted using the Earth Simulator at Japan Agency for Marine-Earth Science and Technology (JAMSTEC) and the EIC parallel computer at the Earthquake Information Center at the Earthquake Research Institute, the University of Tokyo. We thank Barbara Romanowicz, an anonymous reviewer, and the Editor (M. Savage) for their constructive comments, which were very helpful for the revision.

- Denolle, M. A., Dunham, E. M., Prieto, G. A., & Beroza, G. C. (2014). Strong ground motion prediction using virtual earthquakes. *Science*, 343(6169), 399–403. <https://doi.org/10.1126/science.1245678>
- Earthquake-Reports.com (2013). Massive earthquake in Russia's far east—Felt in Moscow and parts of China, India and Japan, <https://earthquake-report.com/2013/05/24/massive-earthquake-sea-of-okhotsk-on-may-24-2013/>.
- Frohlich, C. (2006). *Deep earthquakes*. Cambridge, UK: Cambridge University Press. <https://doi.org/10.1017/CBO9781107297562>
- Furumura, T., & Hayakawa, T. (2007). Anomalous propagation of long-period ground motions recorded in Tokyo during the 23 October 2004 M_w 6.6 Niigata-ken Chuetsu, Japan, Earthquake. *Bulletin of the Seismological Society of America*, 97(3), 863–880. <https://doi.org/10.1785/0120060166>
- Furumura, T., & Kennett, B. L. N. (2005). Subduction zone guided waves and the heterogeneity structure of the subducted plate: Intensity anomalies in northern Japan. *Journal of Geophysical Research*, 110, B10302. <https://doi.org/10.1029/2004JB003486>
- Furumura, T., & Kennett, B. L. N. (2008). A scattering waveguide in the heterogeneous subducting plate. In R. Dmowska (Ed.), *Earth heterogeneity and scattering effects on seismic waves, Advances in Geophysics*, (Vol. 50, pp. 195–217). Amsterdam: Elsevier. [https://doi.org/10.1016/s0065-2687\(08\)00007-1](https://doi.org/10.1016/s0065-2687(08)00007-1)
- Furumura, T., & Kennett, B. L. N. (2017). Unusual strong ground motion across Japan from the 680 km deep 30 May 2015 Ogasawara Islands earthquake. *Journal of Geophysical Research: Solid Earth*, 122, 8143–8162. <https://doi.org/10.1002/2017JB014519>
- Kennett, B. L. N., Engdahl, E. R., & Buland, R. (1995). Constraints on seismic velocities in the Earth from travel times. *Geophysical Journal International*, 122(1), 108–124. <https://doi.org/10.1111/j.1365-246X.1995.tb03540.x>
- Kennett, B. L. N., & Furumura, T. (2015). Toward the reconciliation of seismological and petrological perspectives on oceanic lithosphere heterogeneity. *Geochemistry, Geophysics, Geosystems*, 16, 3129–3141. <https://doi.org/10.1002/2015GC006017>
- Kennett, B. L. N., & Furumura, T. (2019). Significant P wave conversion from upgoing S waves generated by very deep earthquakes around Japan. *Progress in Earth and Planetary Science*, 6(1), 49. <https://doi.org/10.1186/s40645-019-0292-z>
- Koketsu, K., Hatayama, K., Furumura, T., Ikegami, Y., & Akiyama, S. (2005). Damaging long-period ground motions from the 2003 M_w 8.3 Tokachi-oki, Japan earthquake. *Seismological Research Letters*, 76(1), 67–73. <https://doi.org/10.1785/gssrl.76.1.67>
- Koketsu, K., Miyake, H., Fujiwara, H., & Hashimoto, T. (2008). Progress towards a Japan integrated velocity structure model and long-period ground motion hazard map. Proceedings of the 14th World Conference on Earthquake Engineering, S10-038.
- Kuge, K. (2015). Teleseismic peak ground accelerations from the 24 May 2013 Sea of Okhotsk deep earthquake. *Bulletin of the Seismological Society of America*, 105(4), 2058–2069. <https://doi.org/10.1785/0120140315>
- Langston, C. A. (1996). The SsPmp phase in regional wave propagation. *Bulletin of the Seismological Society of America*, 86, 133–143.
- Laske, G., Masters, G., Ma, Z., & Pasyanos, M. (2013). Update on CRUST1.0—A 1-degree global model of Earth's crust. *Geophys. Res. Abstracts*, 15, Abstract EGU2013-2658.
- Maeda, T., Obara, K., Furumura, T., & Saito, T. (2011). Interference of long-period seismic wavefield observed by dense Hi-net array in Japan. *Journal of Geophysical Research*, 116, B10303. <https://doi.org/10.1029/2011JB008464>
- Maeda, T., Takemura, S., & Furumura, T. (2017). OpenSWPC: An open-source integrated parallel simulation code for modeling seismic wave propagation in 3D heterogeneous viscoelastic media. *Earth, Planets and Space*, 69(1). <https://doi.org/10.1186/s40623-017-0687-2>
- Montagner, J.-P., & Kennett, B. L. N. (1996). How to reconcile body-wave and normal-mode reference Earth models. *Geophysical Journal International*, 125(1), 229–248. <https://doi.org/10.1111/j.1365-246X.1996.tb06548.x>
- National Research Institute for Earth Science and Disaster Resilience (2019). NIED Hi-net, National Research Institute for Earth Science and Disaster Resilience, doi:<https://doi.org/10.17598/nied.0003>.
- Oliver, J. (1961). On the long period character of shear waves. *Bulletin of the Seismological Society of America*, 51, 1–12.
- RT (2013). Tremors felt in Moscow as 8.2 quake rattles Russia's Sakhalin region. <http://www.rt.com/news/quake-asia-tsunami-warning-729/>
- U.S. Geological Survey (USGS) (2013). M8.3—Sea of Okhotsk, 2013-05-24 05:44:48 (UTC) 54.892°N 153.221°E 598.1 km depth, Did You Feel It?. <https://earthquake.usgs.gov/earthquakes/eventpage/usb000h4jh/dyfi/intensity>.
- Vidale, J. E. (1987). Waveform effects of a high-velocity, subducted slab. *Geophysical Research Letters*, 14(5), 542–545. <https://doi.org/10.1029/GL014i005p00542>
- Wei, S., Helmlinger, D., Zhan, Z., & Graves, R. (2013). Rupture complexity of the M_w 8.3 sea of Okhotsk earthquake: Rapid triggering of complementary earthquakes? *Geophysical Research Letters*, 40, 5034–5039. <https://doi.org/10.1002/grl.50977>
- Wessel, P., & Smith, W. H. F. (1998). New, improved version of generic mapping tools released. *Eos, Transactions of the American Geophysical Union*, 79(47), 579. <https://doi.org/10.1029/98EO00426>
- Yokota, T., Nemoto, M., Matsusue, K., Takase, S., Takata, K., & Ikeda, M. (2017). Study on the plate model of the Pacific plate. Abstract of JpGU-AGU Joint Meeting, 2017, SSS13-P04.